Electronic Supplementary Material (ESI) for Journal of Materials Chemistry C.

Supplementary Information

A dual-response regenerable luminescent 2D-MOF for nitroaromatic sensing via target-modulation of active interaction sites

Farzaneh Afshariazar, Ali Morsali*

Department of Chemistry, Faculty of Sciences, Tarbiat Modares University, P.O. Box 14115-175, Tehran, Iran

E-mail: Morsali_a@modares.ac.ir

Experimental section.

Materials and characterization techniques.

All chemical materials were commercially available and used as received. Infrared spectra were recorded using a Thermo Scientific Nicolet IR 100 FT-IR spectrometer. X-ray powder diffraction (XRD) measurements were done on a Philips X'pert diffractometer with monochromated Cu-Kα radiation. Thermal curves were obtained on a PL-STA 1500 apparatus with the heating rate of 10ºC /min up to 800 ºC under a constant flow of nitrogen. SEM analysis was performed by TESCAN MIRA instrument. Sonochemical synthesis was carried out in a SONICA-2200 EP ultrasonic bath (frequency of 20 kHz). The luminescent properties were investigated by a fluorescence spectrometer (PerkinElmer LS45) with a slit width of 10 nm at ambient conditions.

Table S1. Structural data and refinement parameters for **TMU-58**.[1]

Crystal data	
Chemical formula	C_{31} H_{27} N_7 O_6 Zn
M_r	658.97
Crystal system	Monoclinic
Space group	$P2_1/c$
Temperature [K]	298(2)
a [Å]	9.248(2)
b [Å]	26.079(6)
c [Å]	12.051(3)
α [˚]	90.0
β [˚]	96.937(6)
γ [˚]	90.0
V [Å]^3	2885.3(12)
Z	4
μ [mm^{-1}]	0.910
Data collection	
T_{min}, T_{max}	0.8044, 0.8533
No. of measured reflections	23321
No. of independent reflections	5646
No. of observed reflections [I > 2σ(I)]	4141
R_{int}	0.0696
θ range for cell measurement	2.31 to 24.08°
Refinement	
$R[F^2 > 2\sigma(F^2)]$	0.0497
$wR(F^2)$	0.1072
S	1.043
No. of reflections	5646
No. of parameters	409
No. of restraints	0
$\Delta\rho_{max}$, $\Delta\rho_{min}$ (e Å^{-3})	0.001, 0.000
CCDC Number	1901306

Table S2. Selected bond distances [Å], and angles [˚] of **TMU-58.**[1]

Zn1 O1	2.001(2)
Zn1 N1	2.065(3)
Zn1 O4	2.172(3)
Zn1 O5	2.118(3)
Zn1 N6	2.085(3)
O1 Zn1 O4	152.8(1)
O1 Zn1 N1	100.2(1)
O1 Zn1 O5	105.1(1)
O4 Zn1 O5	60.9(1)
O4 Zn1 N6	91.0(1)
N1 Zn1 O1	109.1(3)

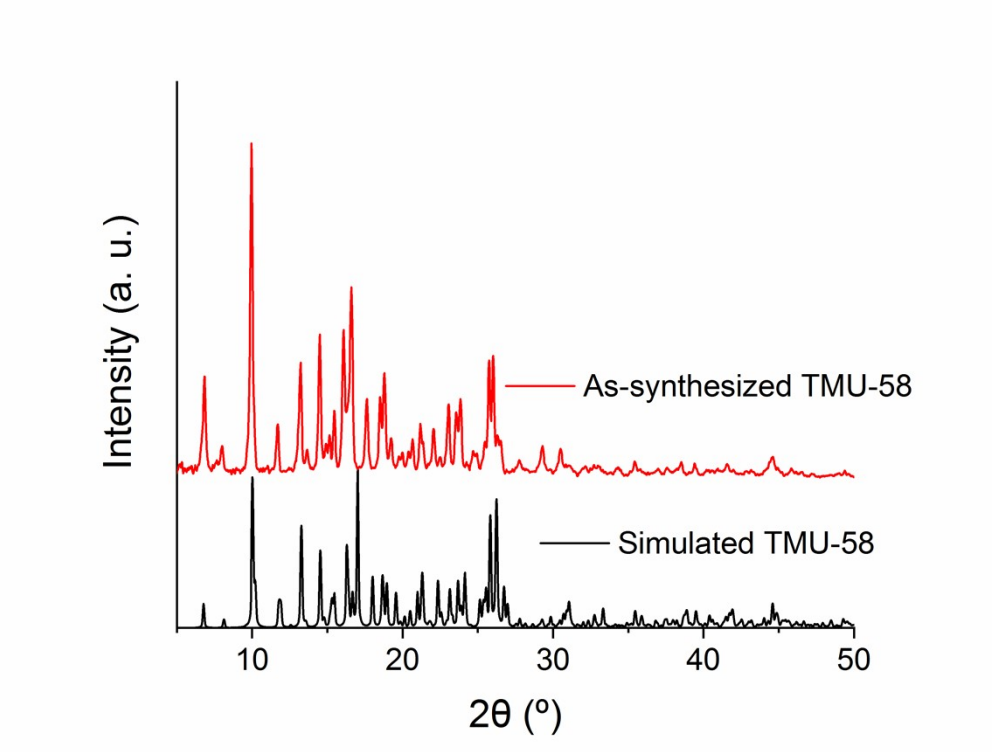

Figure S1- PXRD pattern of **TMU-58**.

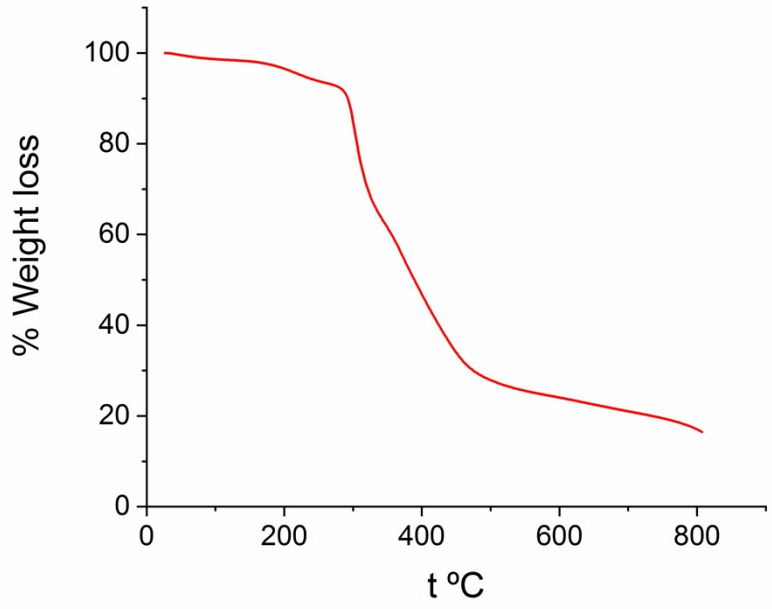

Figure S2. Thermogravimetric analysis of **TMU-58**.

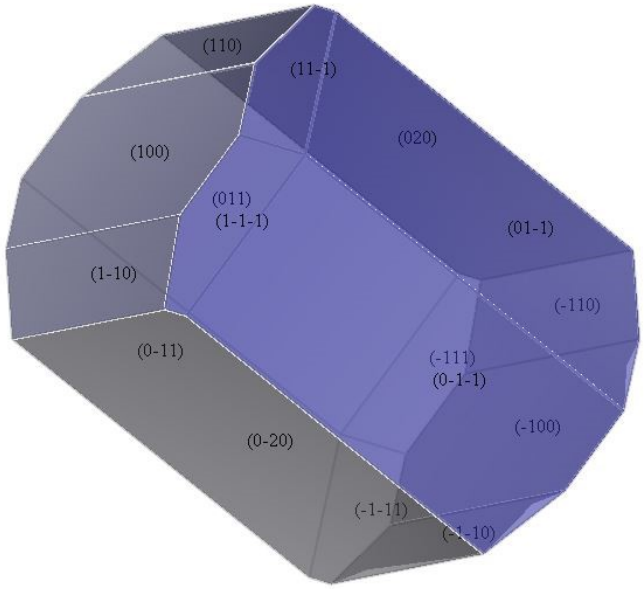

Figure S3. Predicted morphology of **TMU-58** from BFDH analysis.

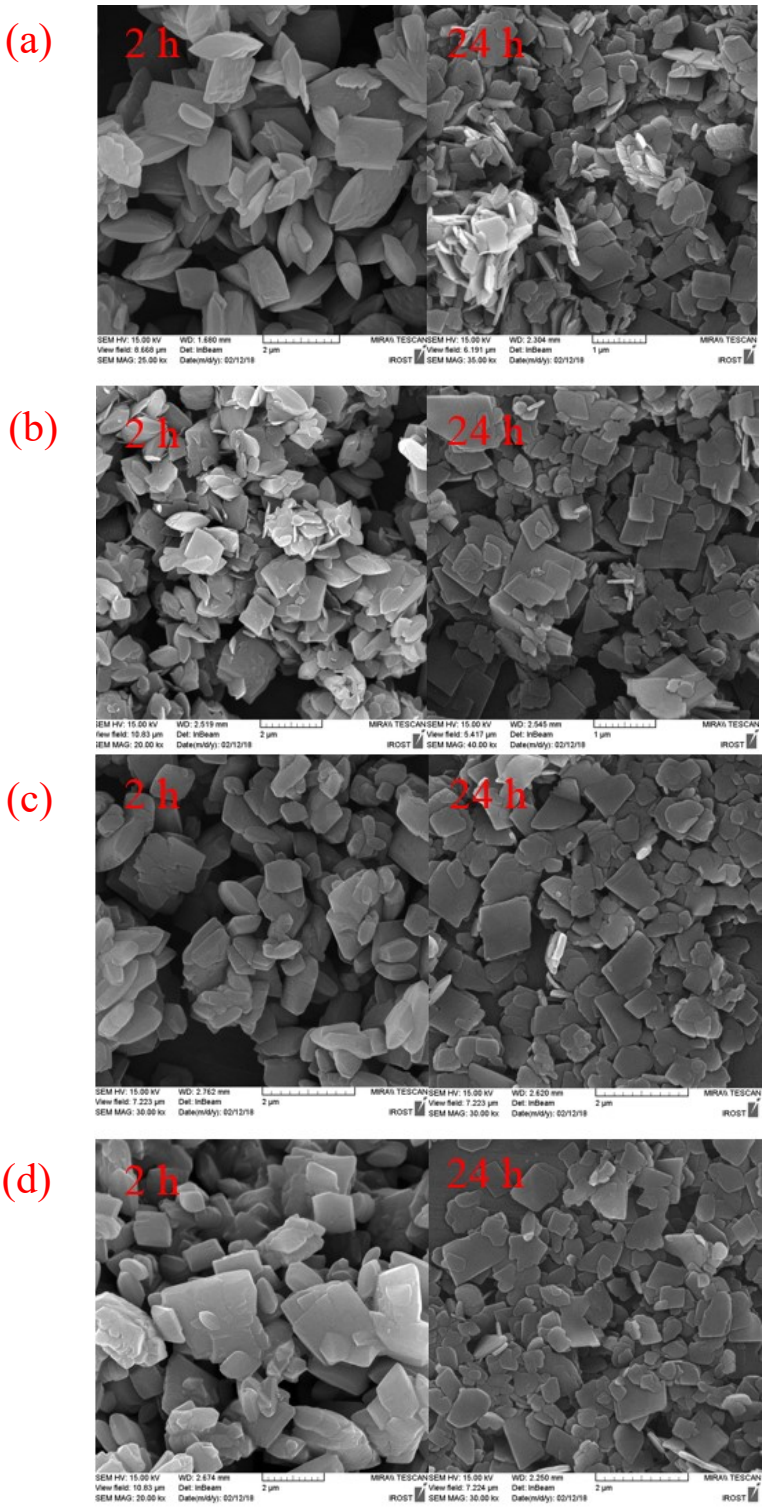

Figure S4. SEM images of **TMU-58** obtained by various concentration of acetic acid to H_2oba ligand (r value) as capping agent. (a) r = 2, (b) r = 5, (c) r = 10, (d) r = 15.

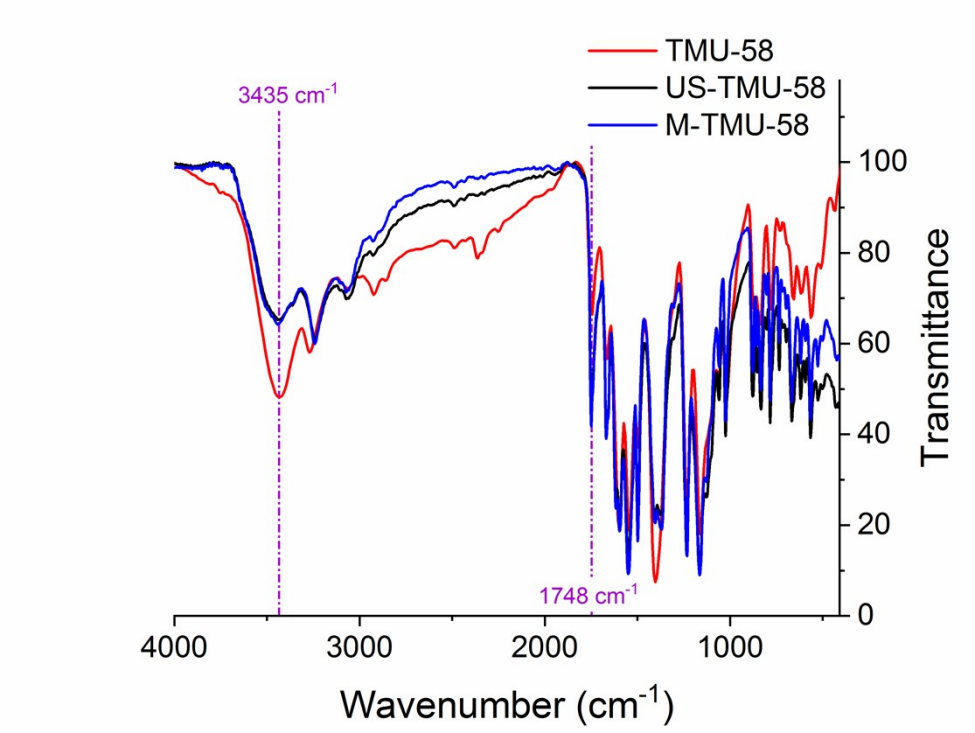

Figure S5. IR spectrum of **TMU-58**, **US-TMU-58**, and **M-TMU-58**.

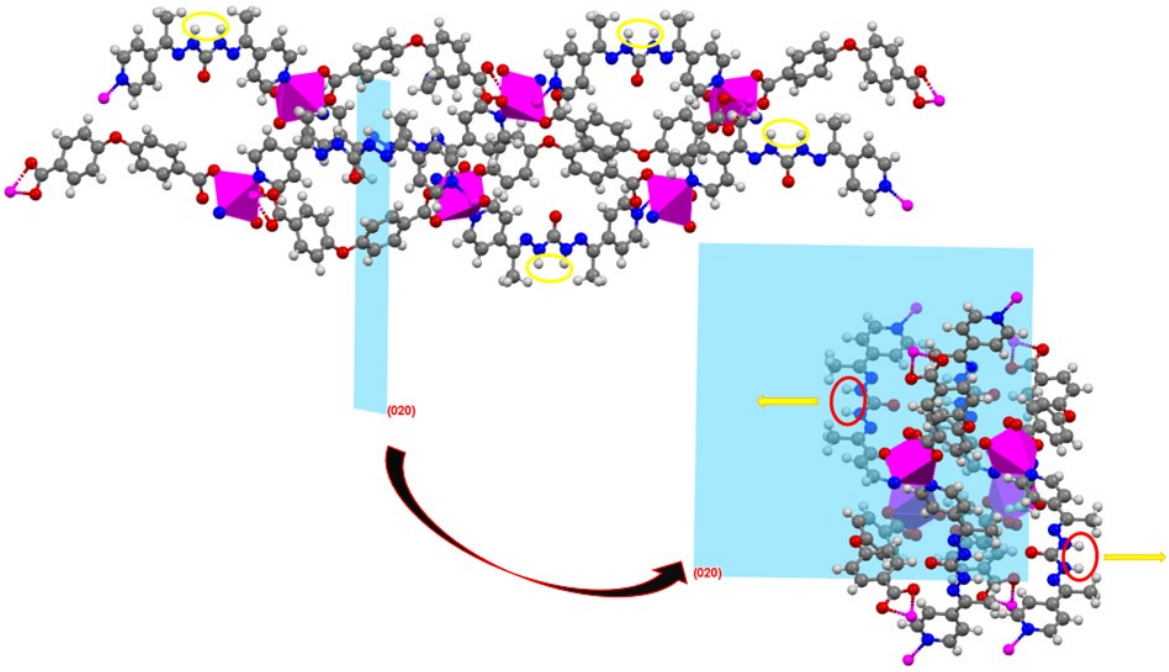

Figure S6. Representation of a 2D-layer of **TMU-58** along the (020) reflection plane.

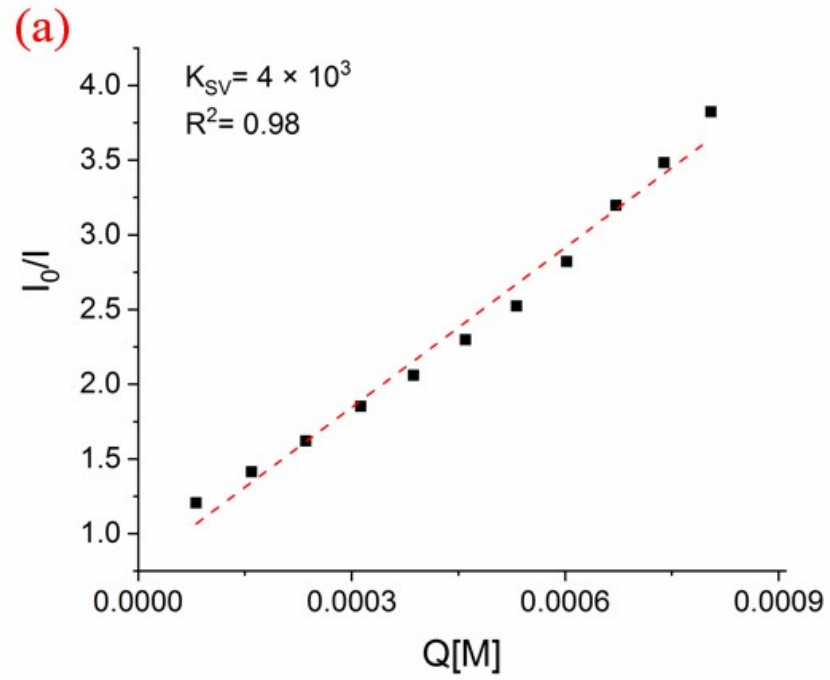
(a)
K_{SV}= 4 × 10^3
R^2= 0.98
I_0/I
4.0
3.5
3.0
2.5
2.0
1.5
1.0
0.0000
0.0003
0.0006
0.0009
Q[M]

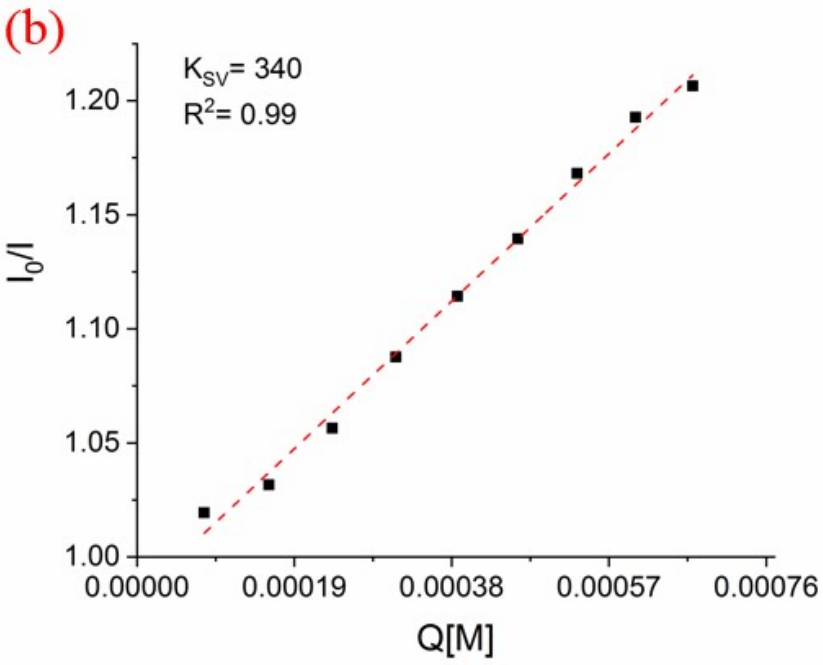
(b)
K_{SV}= 340
R^2= 0.99
I_0/I
1.20
1.15
1.10
1.05
1.00
0.00000
0.00019
0.00038
0.00057
0.00076
Q[M]

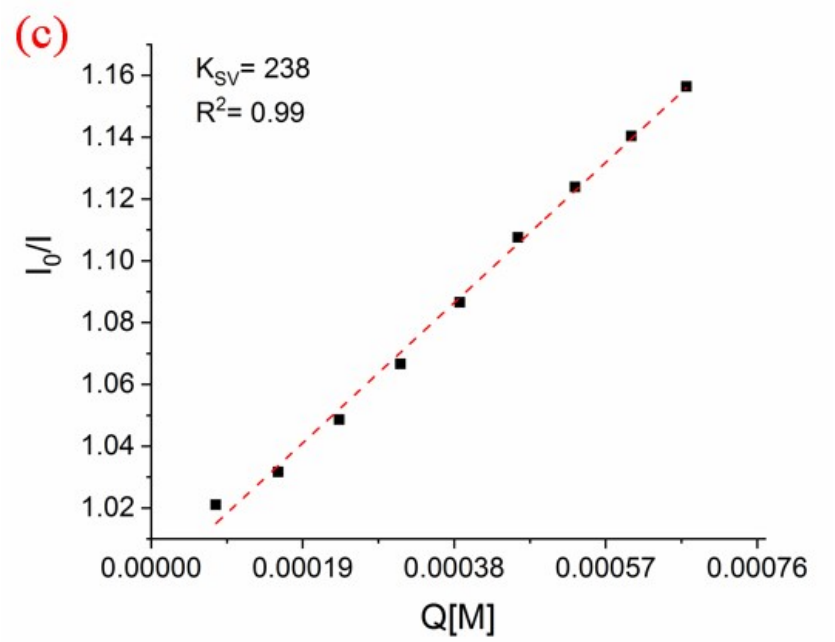

Figure S7. Stern-Volmer plots of a) **TMU-58**, b) **US-TMU-58**, c) **M-TMU-58** for **NB** analyte.

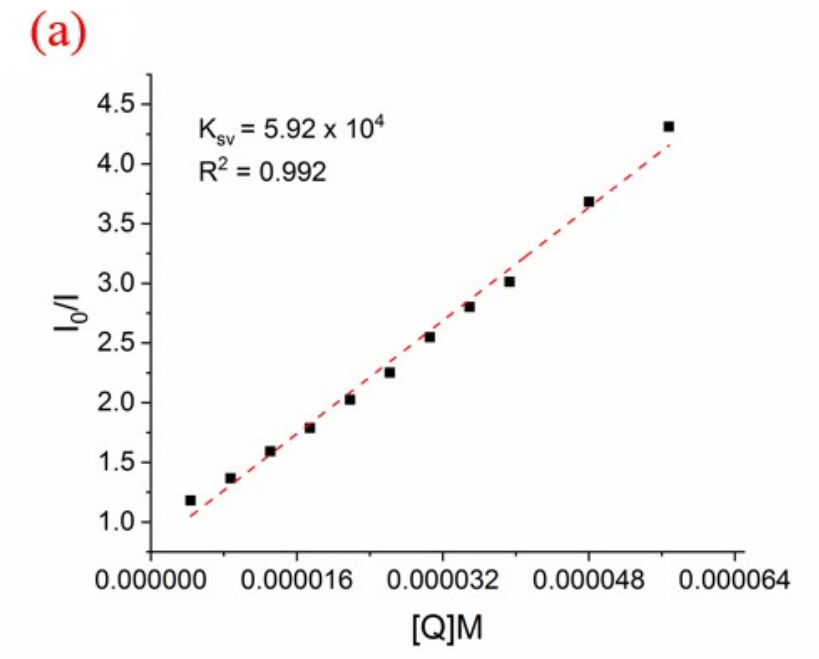

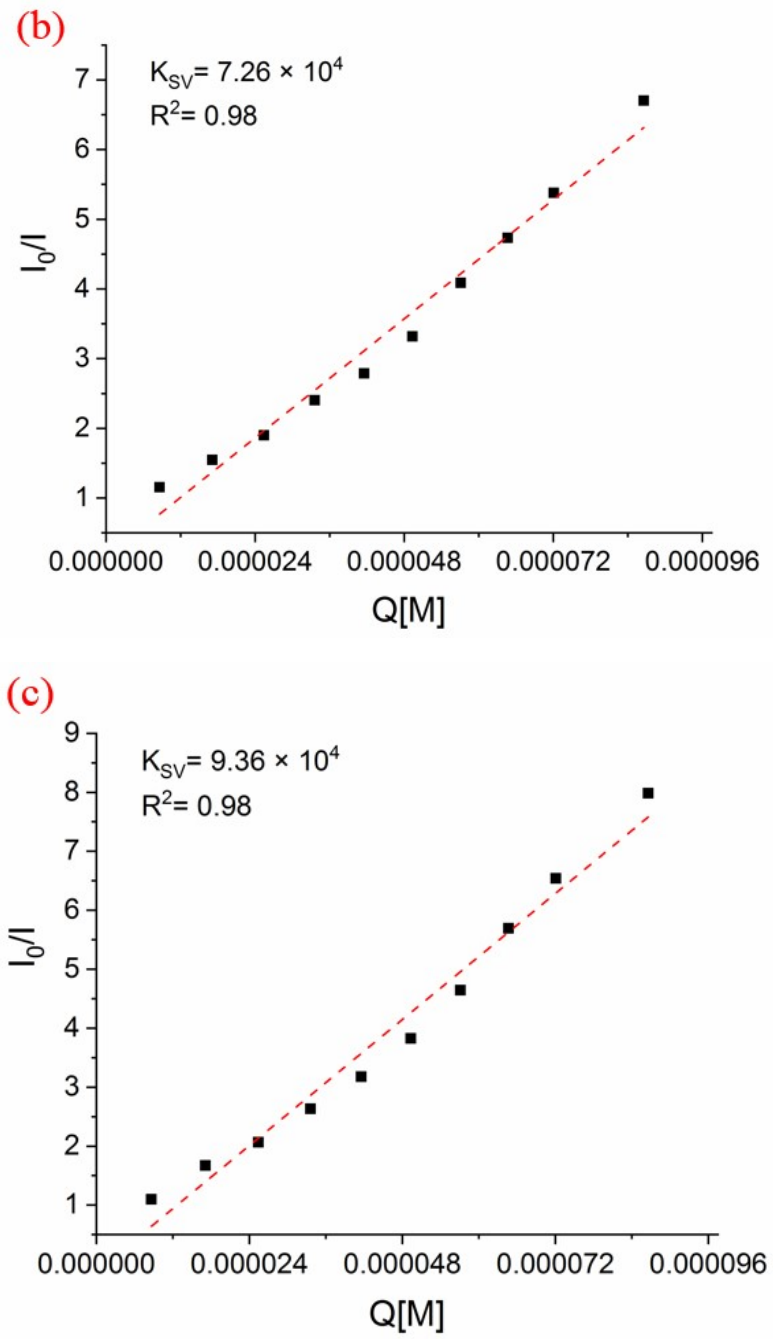

Figure S8. Stern-Volmer plots of a) **TMU-58**, b) **US-TMU-58**, c) **M-TMU-58** for **TNP** analyte.

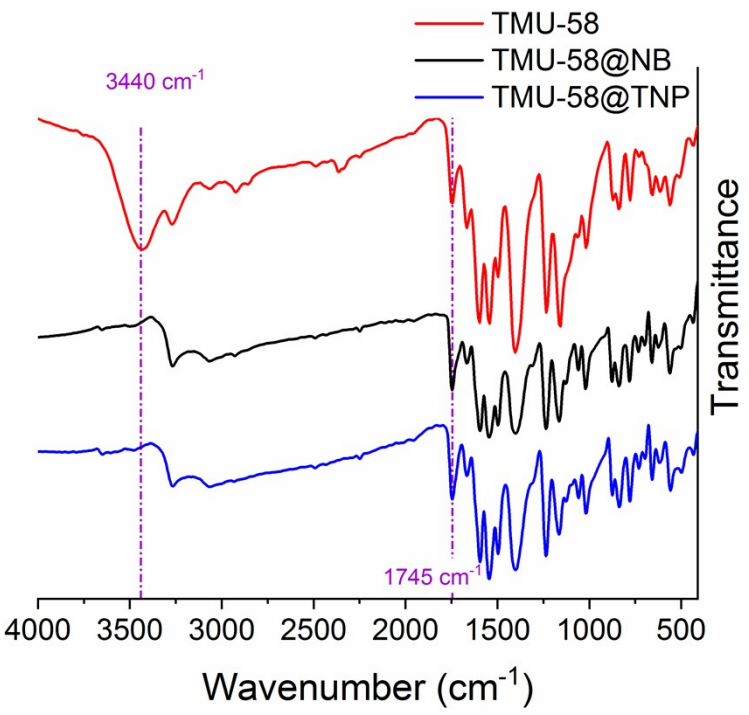

Figure S9. IR spectrums of **TMU-58** before and after sensing of **NB** and **TNP** analytes.

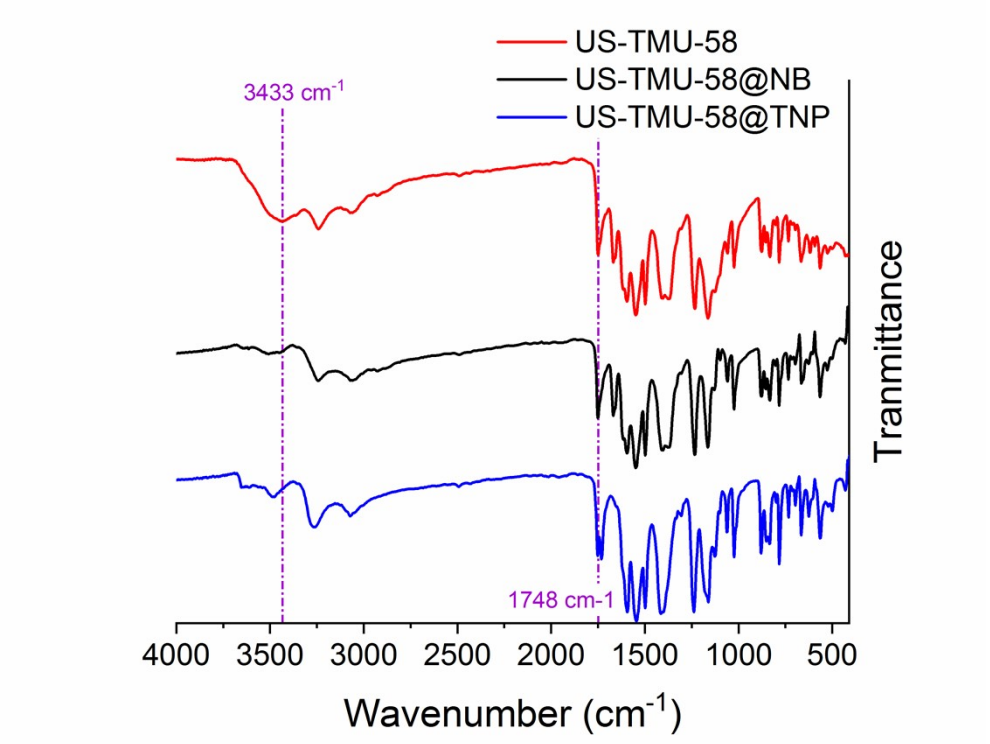

Figure S10. IR spectrums of **US-TMU-58** before and after sensing of **NB** and **TNP** analytes.

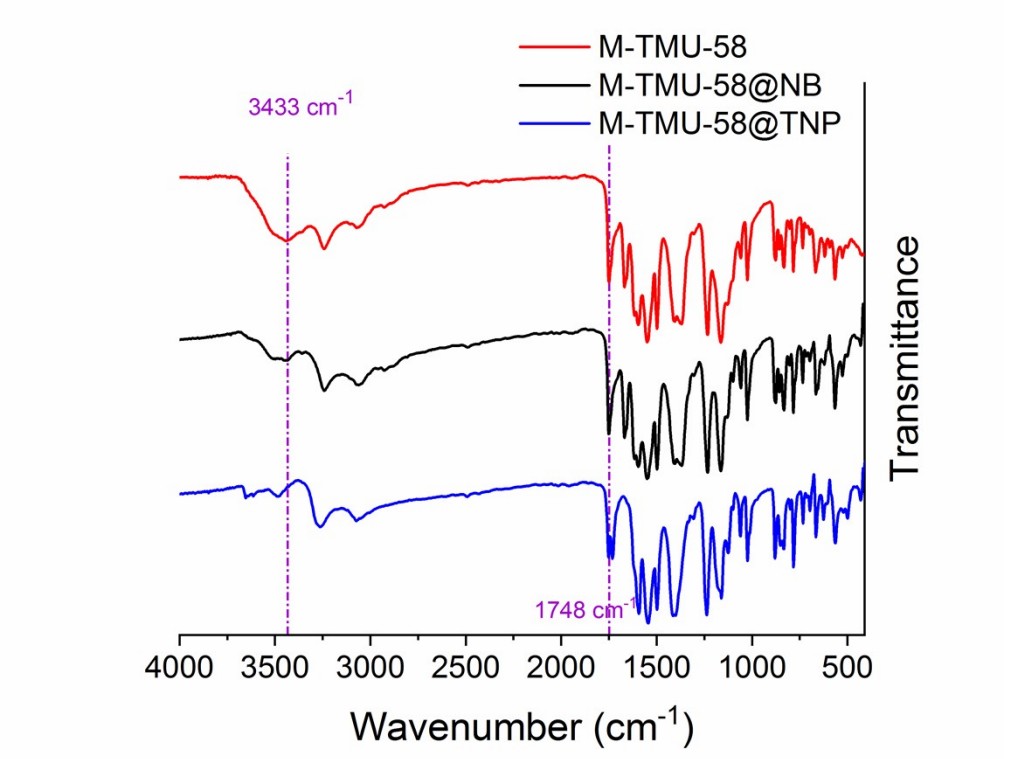

Figure S11. IR spectrums of **M-TMU-58** before and after sensing of **NB** and **TNP** analytes.

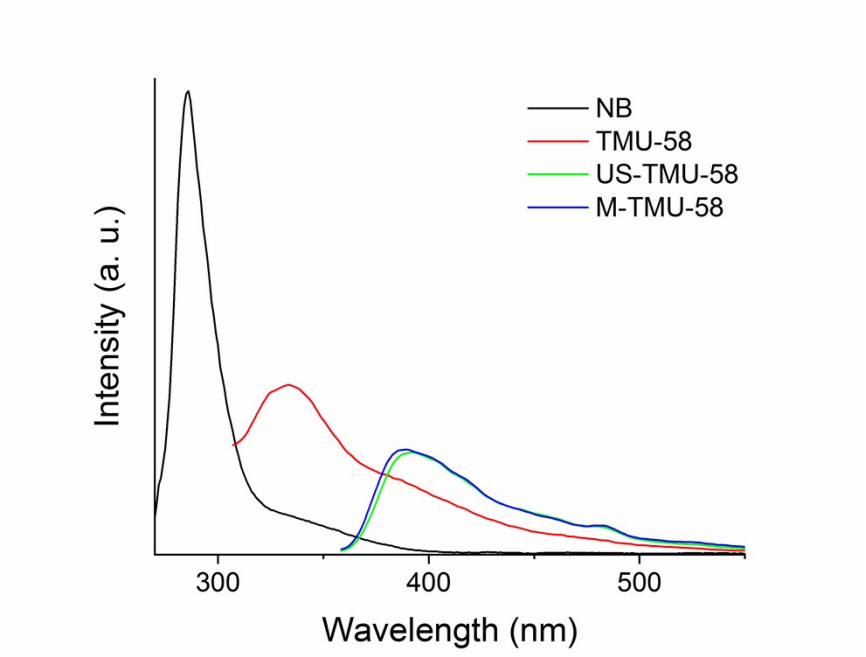

Figure S12. Spectral overlap between the absorption spectra of **NB** analyte and the emission spectrum of **TMU-58**, **US-TMU-58**, and **M-TMU-58**, respectively.

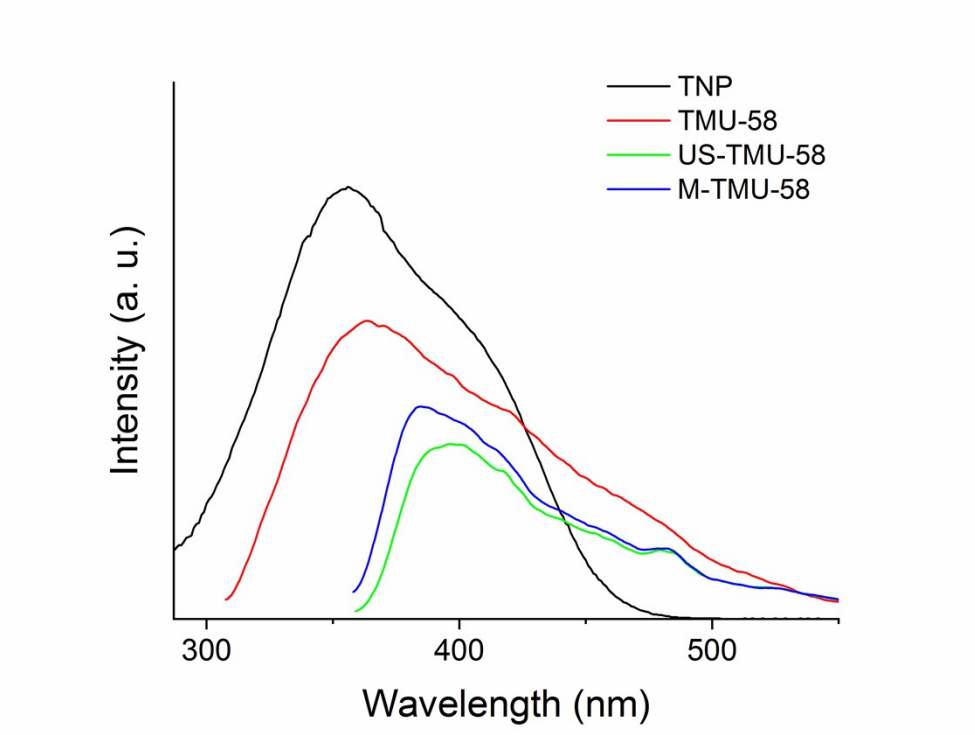

Figure S13. Spectral overlap between the absorption spectra of **TNP** analyte and the emission spectrum of **TMU-58**, **US-TMU-58**, and **M-TMU-58**, respectively.

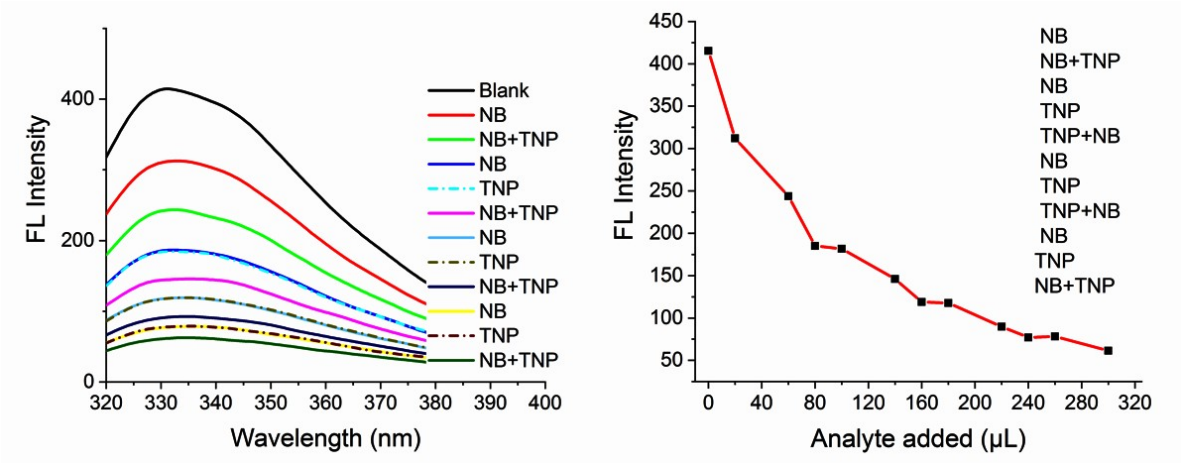

Figure S14. Representation of the response selectivity of **TMU-58** towards **NB** analyte in the presence of **TNP**.

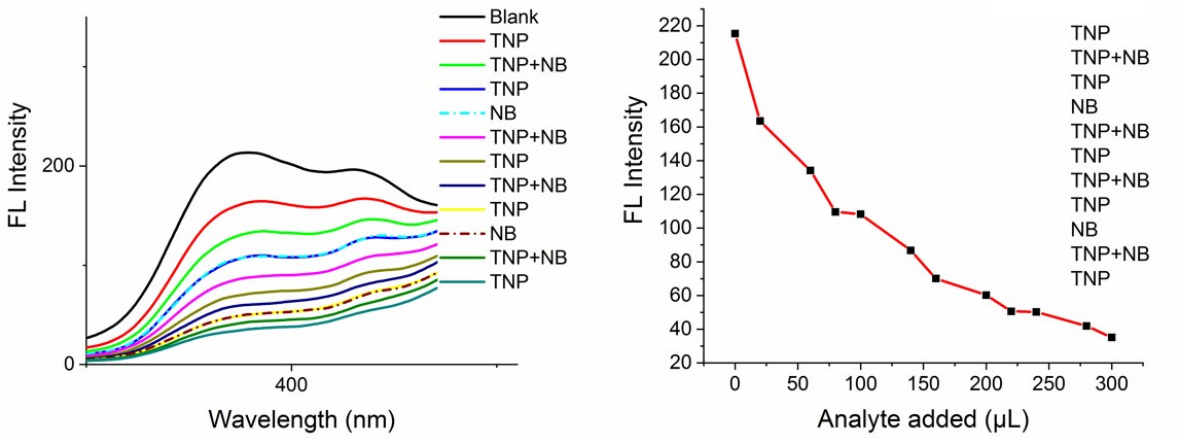

Figure S15. Representation of the response selectivity of **US-TMU-58** towards **TNP** analyte in the presence of **NB**.

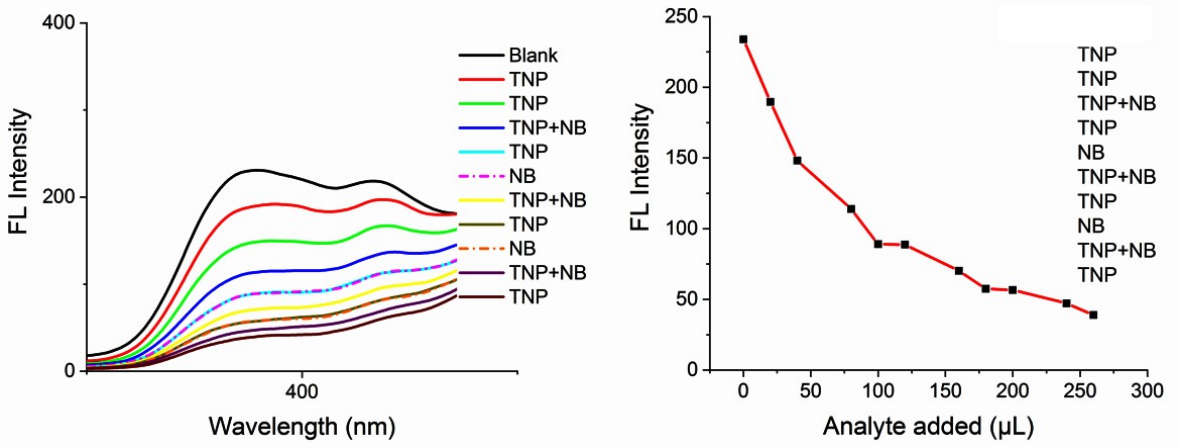

Figure S16. Representation of the response selectivity of **M-TMU-58** towards **TNP** analyte in the presence of **NB**.

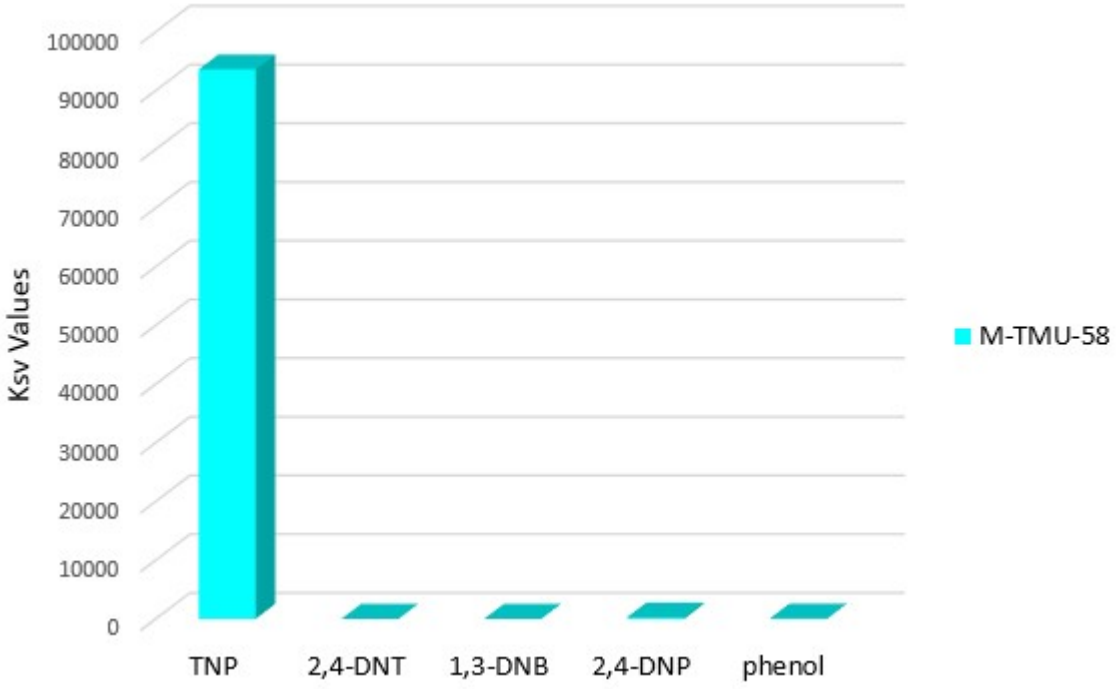

Figure S17. The response selectivity of **M-TMU-58** towards various analytes.

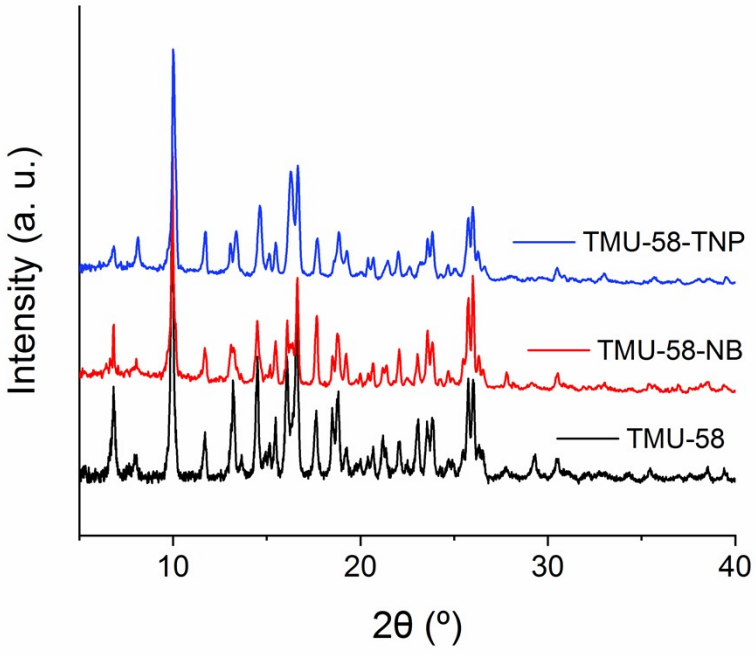

Figure S18. Chemical stability of **TMU-58** after **NB** and **TNP** sensing.

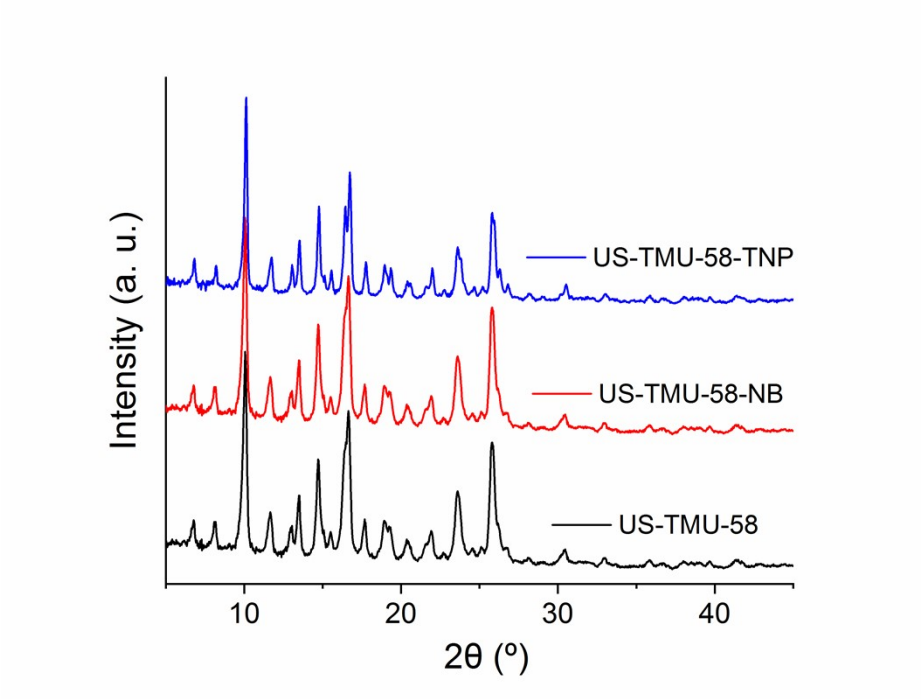

Figure S19. Chemical stability of **US-TMU-58** after **NB** and **TNP** sensing.

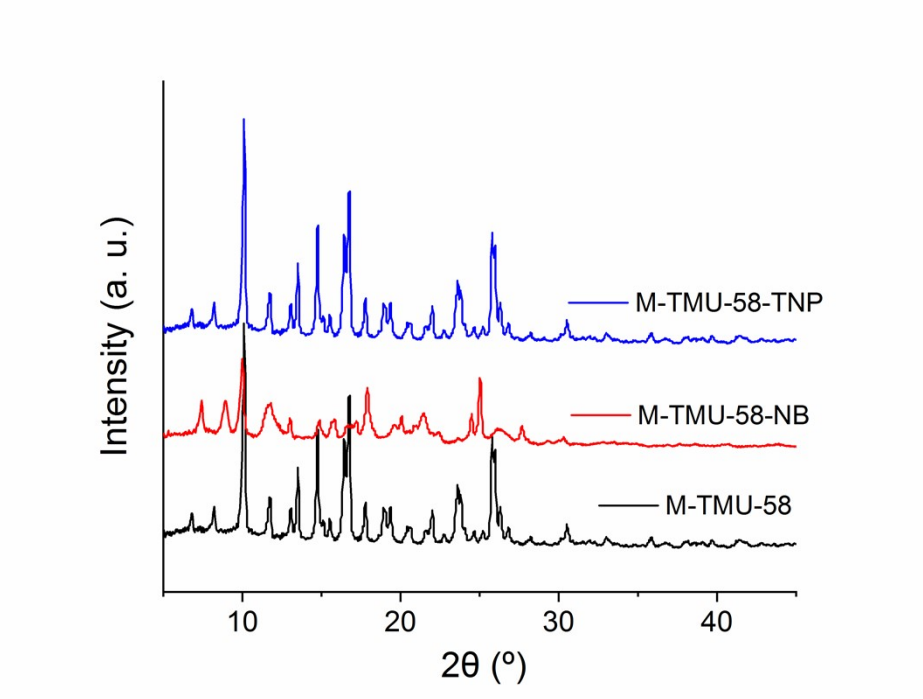

Figure S20. Chemical stability of **M-TMU-58** after **NB** and **TNP** sensing.

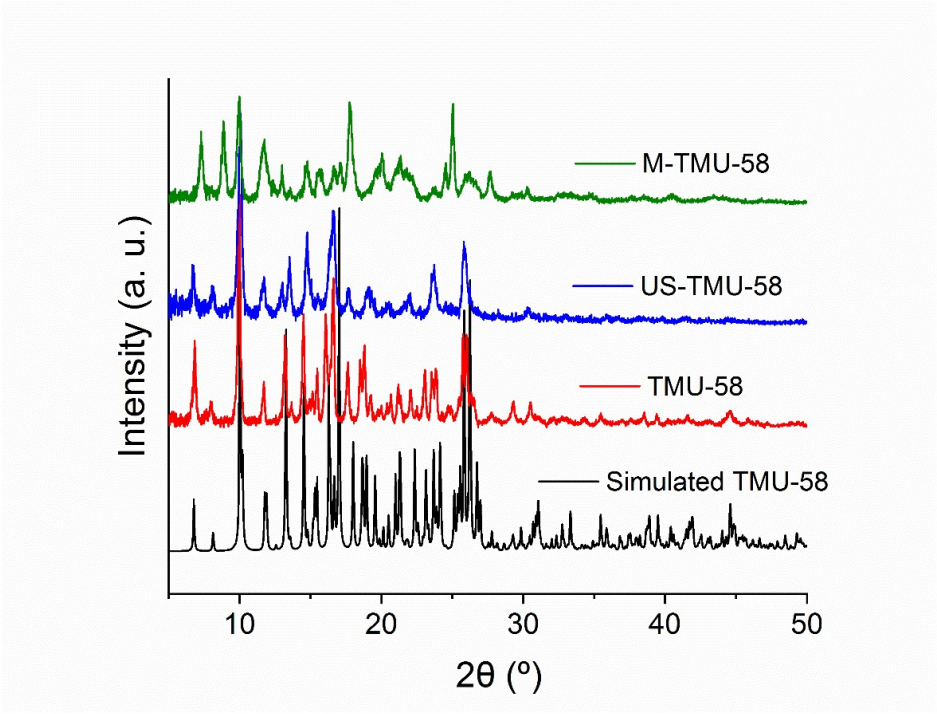

Figure S21. PXRD patterns of recovered **TMU-58**, **US-TMU-58**, and **M-TMU-58** after 3 cycles of sensing.

Reference

1. F. Afshariazar and A. Morsali, Target-Architecture Engineering of a Novel Two-dimensional Metal-Organic Framework for High Catalytic Performance, *Cryst. Growth Des.*, 2019, **19**, 4239–4245.